Title
The effects of disorder on the normal state and superconducting properties of Nb3Sn

Journal
Superconductor Science and Technology, 30(2)

ISSN
0953-2048

Authors
Mentink, MGT
Dhalle, MMJ
Dietderich, DR
et al.

Publication Date
2017-02-01

DOI
10.1088/1361-6668/30/2/025006

Peer reviewed

Superconductor Science and Technology

PAPER

The effects of disorder on the normal state and superconducting properties of Nb_3Sn

To cite this article: M G T Mentink *et al* 2017 *Supercond. Sci. Technol.* **30** 025006

IOP Publishing Superconductor Science and Technology
Supercond. Sci. Technol. 30 (2017) 025006 (13pp) doi:10.1088/1361-6668/30/2/025006

The effects of disorder on the normal state and superconducting properties of Nb_3Sn

M G T Mentink[1], M M J Dhalle[2], D R Dietderich[3], A Godeke[4], F Hellman[5] and H H J ten Kate[1,2]

[1] CERN, CH-1211 Geneva 23, Switzerland
[2] University of Twente, Enschede 7500 AE, the Netherlands
[3] Lawrence Berkeley National Laboratory, 1 Cyclotron Rd, MS 47R0112, Berkeley, CA 94720, USA
[4] National High Field Laboratory, 1800 E Paul Dirac Dr., Tallahassee, FL 32310-3706, USA
[5] University of California, Berkeley, 366 LeConte Hall MC 7300, Berkeley, CA 94720-7300, USA

E-mail: mmentink@cern.ch

Received 25 August 2016, revised 24 October 2016
Accepted for publication 2 November 2016
Published 13 December 2016

Abstract

The effect of disorder on the normal state resistivity and the superconducting properties of Nb_3Sn is explored in a combination of *ab initio* calculations and microscopic theory. The crystal symmetry is calculated to be preferentially tetragonal at a normal state resistivity below 27.0 ± 1.4 $\mu\Omega$cm, and preferentially cubic above this value, which is shown to be consistent with the experimentally observed transition point. The phonon density of states, the Eliashberg spectrum $\alpha^2(\omega)F(\omega)$, the electron–phonon coupling constant, the characteristic frequency, the critical temperature T_c, and the upper critical magnetic field at 0 K $H_{c2}(0)$ are calculated over a large normal state resistivity range and shown to be consistent with experimental observations. The high degree of consistency between the calculation results and experimental observations is a strong indication that the calculation approach utilized here, a combination of *ab initio* calculations and microscopic theory, is a useful tool for understanding the superconducting and normal state properties of Nb_3Sn.

Keywords: Nb_3Sn, microscopic theory, superconducting properties

1. Introduction

Since the discovery of superconductivity in Nb_3Sn by Matthias *et al* [1] in 1954, this material has attracted a significant amount of scientific attention, not just because of the exotic properties of the material, but also for the suitability of the material for large-scale high-magnetic field applications, such as the high luminosity large hadron collider, the international thermonuclear experimental reactor, nuclear magnetic resonance magnets, and high-magnetic field facilities. Nb_3Sn is well suited for these applications because Nb_3Sn wires can be produced and bundled into cables in a reliable and relatively affordable manner. The superconducting properties of Nb_3Sn exceed the superconducting properties of NbTi, which is another commonly used superconductor for medium-magnetic field applications.

In spite of previous scientific research spanning several decades, the superconductor Nb_3Sn still has features that are not yet fully understood, such as the profound degree by which strain affects the superconducting properties of the material. In addition to strain, the degree of disorder also strongly affects the superconducting properties of Nb_3Sn (see for instance Orlando *et al* [2]). In this paper, a number of phenomena of Nb_3Sn are considered, which include the preferential crystal symmetry, the Eliashberg spectra, the critical temperature, and the upper critical magnetic field as a function of disorder. The behavior is calculated through the use of *ab initio* calculations and subsequently validated through previously published experimental observations. The purposes of this work are to provide a thorough review of existing literature on the microscopic properties of Nb_3Sn, to combine microscopic theory with density functional theory (DFT) calculations, and to validate calculation results for the purpose of demonstrating the applicability of the approach for understanding the exotic properties of Nb_3Sn. For future purposes, the calculation approach taken here could be used to investigate specific phenomena of superconducting Nb_3Sn,

such as the large intrinsic strain sensitivity of its superconducting properties (also see [3]).

Firstly, three starting assumptions are discussed in section 2. Secondly, a variety of calculation results pertaining to normal state properties of Nb_3Sn are compared to experimental observations in section 3 for the purpose of providing empirical validation for assumptions given in section 2. This comparison includes results regarding the martensitic transformation, the electron density of states, the Fermi velocity, the phonon density of states, the Eliashberg spectrum, the electron–phonon coupling constant, and the characteristic phonon frequency. Thirdly, calculation results are shown side-by-side with experimental observations on the superconducting phase boundary in section 4, which include the critical temperature, the upper critical field and a discussion on the influence of the martensitic transformation on the critical temperature and upper critical field. Finally, this is followed by a discussion in section 5 and conclusions in section 6.

2. Starting assumptions

2.1. Assumption #1: electron lifetime broadening approximation

In order to study the influence of disorder in the *ab initio* calculations, a previously published concept after Testardi and Mattheiss [4, 5] was used. In this concept, disorder is introduced through electron lifetime broadening. The underlying idea is that the energy of an electron in a disordered material is poorly defined in comparison to the energy of an electron in a perfect crystal, because the electron in the disordered material scatters more often. The degree of uncertainty, i.e. broadening, is expressed with [5]:

$$E_b = \frac{\hbar}{\tau}, \tag{1}$$

where E_b is the broadening energy in (eV), $\hbar$ is the reduced Planck constant in (eV $\times$ s), and τ is the mean scattering time in (s). Thus, disorder is incorporated through a mean scattering time τ, where a smaller τ indicates a higher degree of disorder.

This broadening term is subsequently introduced in DFT and density functional perturbation theory (DFPT) calculations, through which the effect of disorder on a stoichiometric unit cell, i.e. two Sn ions and six Nb ions, is investigated.

The validity of this assumption is empirically demonstrated through a variety of comparisons between calculation results and experimental observations, in particular with regards to the disorder-dependent occurrence of the martensitic transformation in section 3.2.

2.2. Assumption #2: empirical $\alpha^2(\omega)$ dependence

A second underlying assumption involves the electron–phonon coupling characteristic α^2. The relevance of $\alpha^2(\omega)$ is that it relates the electron–phonon coupling constant λ to the electronic and vibrational properties of the material. λ is related to the phonon density of states $F(\omega)$ through [6]:

$$\lambda = 2\int \frac{\alpha^2(\omega)F(\omega)}{\omega}\delta\omega, \tag{2}$$

where $\alpha^2(\omega)$ is the electron–phonon coupling characteristic, ω the vibrational frequency, and $F(\omega)$ the phonon density of states. It was empirically demonstrated by Markiewicz [7] that, in stoichiometric Nb_3Sn, $\alpha^2(\omega)$ is proportional to an exponential function:

$$\alpha^2(\omega) = \alpha_0 \exp(-\omega/\omega_0), \tag{3}$$

where ω_0 is a characteristic frequency and α_0 is a constant. Analogous to the method as used by Markiewicz, $\alpha^2(\omega)$ was determined from published measurements of the Eliashberg spectrum $\alpha^2(\omega)F(\omega)$ (after Rudman *et al* [8], Shen [9], Geerk *et al* [10], Freeriks *et al* [11], and Wolf [12]) and the phonon density of states $F(\omega)$ (after Schweiss *et al* [13]), as shown in figure 1. These results are then fitted with equation (3) to find a value of 14.2 meV for ω_0 and 32.0 meV for α_0.

According to McMillan [14] and Hopfield [15] λ is proportional to the electron density of states $N(E_F)$ through:

$$\lambda = \frac{N(E_F)\langle I^2\rangle}{\langle\omega^2\rangle M}, \tag{4}$$

where $\langle I^2\rangle$ is the mean electronic matrix element, M the effective ion mass, and $\langle\omega^2\rangle$ the average of the squared vibrational frequency in the Eliashberg spectrum. The phonon density of states is a normalized quantity, i.e.:

$$\int F(\omega)\delta\omega \equiv 1. \tag{5}$$

The definition of $\langle\omega^2\rangle$ is as follows:

$$\langle\omega^2\rangle \equiv \frac{2}{\lambda}\int \alpha^2(\omega)F(\omega)\omega \times \delta\omega. \tag{6}$$

When combining equations (2), (4)–(6), a solution for $\alpha^2(\omega)$ is found for a material with a single ion species:

$$\alpha^2(\omega) = \frac{\langle I^2\rangle}{2M}\frac{N(E_F)}{\omega} = \alpha^2_{IM}\frac{N(E_F)}{\omega}, \tag{7}$$

where α^2_{IM} is a constant. However, Nb_3Sn contains two different ion species. As argued by Schweiss [13], λ can be approximated as the sum of the contributions of the various ions, through:

$$\lambda_{eff} = \lambda_1 + \lambda_2 + \cdots. \tag{8}$$

The total phonon density of states is expressed as a sum of the projected phonon densities of states, i.e. the sum of contributions from individual ions:

$$F(\omega) = F_1(\omega) + F_2(\omega) + \cdots. \tag{9}$$

The effective electron–phonon coupling characteristic may then be expressed in terms of the various constituents, with:

$$\alpha^2_{eff}(\omega)F(\omega) = \frac{N(E_F)}{\omega}(\alpha^2_{IM1}F_1(\omega) + \alpha^2_{IM2}F_2(\omega) + \cdots), \tag{10}$$

$$\alpha^2_{eff}(\omega) = \frac{N(E_F)}{\omega}\frac{\alpha^2_{IM1}F_1(\omega) + \alpha^2_{IM2}F_2(\omega) + \cdots}{F(\omega)}. \tag{11}$$

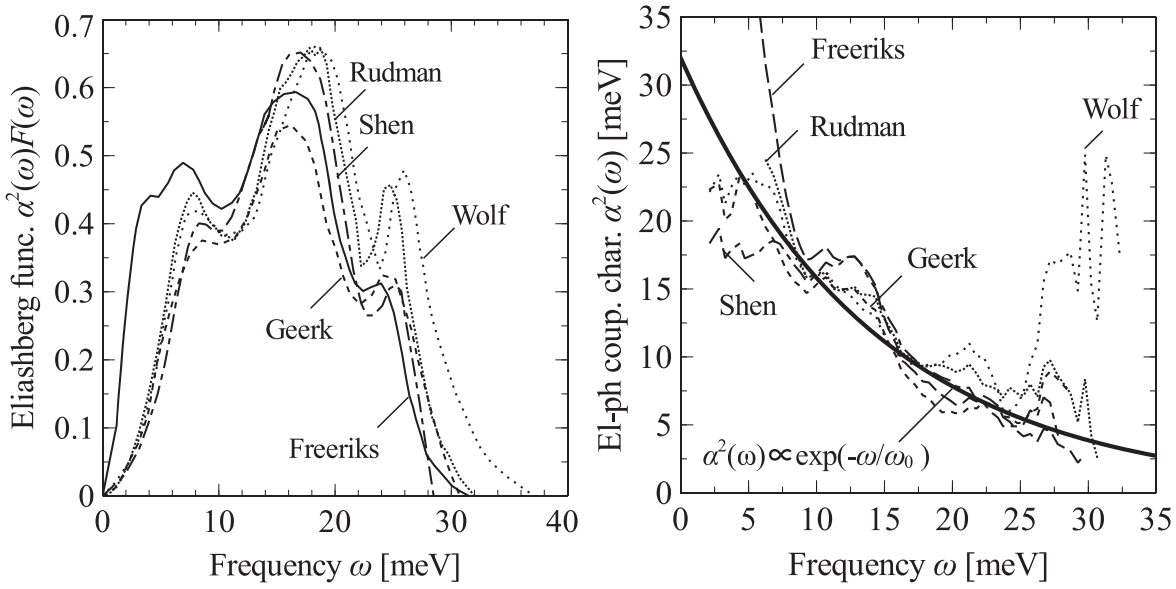

Figure 1. Left: experimentally observed Eliashberg function $\alpha^2(\omega)F(\omega)$ as a function of vibrational frequency ω of low-resistivity Nb_3Sn, determined from stoichiometric tunnel junctions, after Freeriks *et al* [11], Rudman *et al* [8], Shen [9], Geerk *et al* [10], and Wolf [12]. Right: experimentally observed Eliashberg function divided by phonon density of states, after Schweiss *et al* [13], and empirical exponential fit.

A key point is that while equation (7) implies that α^2 may be expressed with a simple analytical equation, in the case of multiple ion species α^2 depends on the relative contributions of the various ions, so that an analytical deduction is no longer trivial. To account for the relative contributions of the various ions, a weighting function is introduced:

$$\alpha^2_{\mathrm{IM,eff}} f(\omega) = \frac{\alpha^2_{\mathrm{IM1}} F_1(\omega) + \alpha^2_{\mathrm{IM2}} F_2(\omega) + \cdots}{F(\omega)}, \tag{12}$$

$$\alpha^2_{\mathrm{eff}}(\omega) = \frac{N(E_{\mathrm{F}})}{\omega} \alpha^2_{\mathrm{IM,eff}} f(\omega). \tag{13}$$

Here $\alpha^2_{\mathrm{IM,eff}}$ is a constant related to the effective ion mass and the mean electronic matrix element and $f(\omega)$ is a weighting function.

The value of $N(E_{\mathrm{F}})$ of stoichiometric Nb_3Sn is taken at 15.4 states/(eV $\times$ unit cell) according to Schachinger *et al* [16], which is consistent with literature results by Orlando *et al* [17] and Ghosh *et al* [18], also see section 3.3. With the given value of $N(E_{\mathrm{F}})$ in stoichiometric Nb_3Sn, the value of $\alpha^2_{\mathrm{IM,eff}}$ and the frequency-dependent $f(\omega)$ may be derived from empirical observations. Combining equations (3) and (13), a value of 2.08×10^{-3} eV^2/(states $\times$ unit cell) is found for $\alpha^2_{\mathrm{IM,eff}}$, and $f(\omega)$ is expressed as:

$$f(\omega) = \omega \exp(-\omega/\omega_0). \tag{14}$$

$f(\omega)$ is a function which peaks at the ω_0, which is equal to 14.2 meV. This result is consistent with the analysis by Schweiss *et al* [13], who pointed out the relatively large contribution of phonons to the intermediate frequency range of the Eliashberg spectrum, and attributed this result to the relatively large degree of electron–phonon coupling of niobium with respect to tin. In other words, Markiewicz's empirical description of the electron–phonon coupling characteristic may be understood in terms of the relative contributions of two different types of ions. Combining equations (13) and (14) we find an empirical expression of $\alpha^2_{\mathrm{eff}}(\omega)$ which is:

$$\alpha^2_{\mathrm{eff}}(\omega) = \alpha^2_{\mathrm{IM,eff}} N(E_{\mathrm{F}}) \exp(-\omega/\omega_0), \tag{15}$$

where $\alpha^2_{\mathrm{IM,eff}}$ is equal to 2.08×10^{-3} eV^2/(states $\times$ unit cell) and ω_0 is equal to 14.2 meV.

To summarize, an attempt was made to analytically derive the expression of α^2_{eff} but it was found that even when α^2 is known for a material with a single ion species, finding an analytical expression for a more complex material such a Nb_3Sn is non-trivial. Therefore, the next best thing is done: to combine microscopic theory with experimental observations on stoichiometric Nb_3Sn and find an empirical expression of $\alpha^2_{\mathrm{eff}}(\omega)$, where $\alpha^2_{\mathrm{IM,eff}}$ and ω_0 are treated as global constants. The validity of this approach is empirically justified in section 3.4.

2.3. Assumption #3: constant effective Coulomb repulsion term μ^*

A third starting assumption pertains to the effective Coulomb repulsion term. The proper value of μ^* is determined in two separate manners.

Firstly, μ^* in both stoichiometric and off-stoichiometric Nb–Sn was previously experimentally determined by Rudman *et al* [8]. From figure 2 it is clear that μ^* stays within the 0.13 ± 0.02 range over the entire normal state resistivity range.

Secondly, the Eliashberg spectra of several stoichiometric low-resistivity Nb_3Sn samples were previously published and the critical temperature of stoichiometric Nb_3Sn is known to be about 18 K. The critical temperature is related to the Eliashberg spectrum and μ^*. Two commonly used expressions, both of which incorporate strong-coupling corrections, are the critical temperature expressions by Kresin

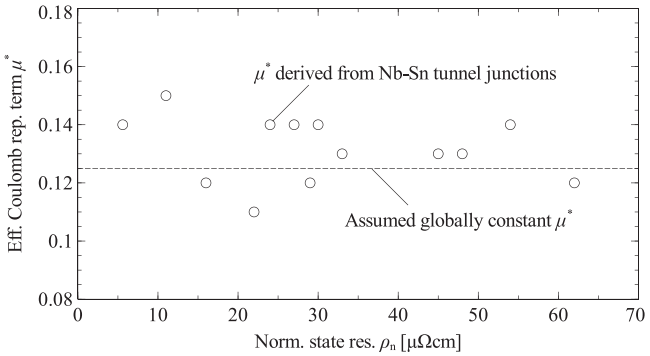

Figure 2. Effective Coulomb repulsion term μ^* as a function of ρ_n of Nb–Sn after Rudman *et al* [8] and assumed globally constant μ^*.

Table 1. Values for λ, $\langle\omega^2\rangle^{0.5}$ and μ^* of weakly disordered stoichiometric Nb_3Sn after Rudman *et al* [8], Shen [9], Geerk *et al* [10], Freeriks *et al* [11], and Wolf [12], mean values, and standard deviations.

	λ	$\langle\omega^2\rangle^{0.5}$ (meV)	μ^*_{Kresin}	$\mu^*_{\text{Allen-Dynes}}$
Freeriks	2.55	10.9	0.17	0.17
Wolf	1.79	15.2	0.16	0.15
Shen	1.56	13.9	0.09	0.11
Geerk	1.50	13.8	0.08	0.06
Rudman	1.75	14.2	0.13	0.12
Average	1.83	13.6	0.127	0.122
Std.dev	0.42	1.6	0.042	0.044

[19] and by Allen and Dynes [20], with:

$$T_{c,\text{Kresin}} = \frac{0.25\,\langle\omega^2\rangle^{0.5}}{\sqrt{e^{2/\lambda_{\text{eff}}} - 1}}, \tag{16}$$

$$T_{c,\text{AD}} = \frac{f_1 f_2\,\omega_{\log}}{1.2}\exp\left(\frac{-1.04(1+\lambda)}{\lambda - \mu^* - 0.62\lambda\mu^*}\right), \tag{17}$$

where λ_{eff}, f_1, f_2, and $\omega_{\log}$ are related to λ, μ^*, and the Eliashberg spectrum. For brevity, the full sets of equations are not reproduced here, but the reader is referred to the original papers.

With both the Eliashberg spectrum and critical temperature of stoichiometric low-resistivity known, the only unknown parameter is μ^*, which may then be calculated for each measurement and each of the two expressions. The result of this is shown in table 1. The average of μ^*, deduced for five published Eliasberg spectrum and using both equations is 0.125, with a standard deviation of 0.04. This value is taken as a global constant, which is found to be consistent with the experimental observations over the entire investigated resistivity range (figure 2).

3. Comparison of calculated versus experimentally observed normal state properties

3.1. DFT and DFPT calculations

With these three assumptions, a series of DFT and DFPT calculations are performed using quantum Espresso [21], an open source software suite for electron-structure calculations. The purpose is to allow for comparisons between calculation results and experimental observations.

DFT and DFPT calculations are performed on a simulated stoichiometric Nb_3Sn unit cell, consisting of six niobium and two tin atoms, which are arranged in the A15 crystal structure (figure 3, left graph). Quantum Espresso uses a plane waves basis set and pseudopotentials. Perdew–Wang 91 gradient corrected functional approximation pseudopotentials [22] are used, and they are readily available on the Quantum Espresso website [23]. All calculations were performed with a kinetic energy cutoff of 40 Rydberg (540 eV) and a charge density cutoff of 320 Rydberg (4350 eV). Structural optimization and density of states calculations were performed with a k-point grid consisting of 16 × 16 × 16 automatic Monkhorst–Pack divisions. Fermi velocity calculations were performed with a k-point grid of 40 × 40 × 40 automatic Monkhorst–Pack divisions. The phonon calculations were performed with a k-point grid consisting of 8 × 8 × 8 Monkhorst–Pack divisions and a q-point grid consisting of 4 × 4 × 4 Monkhorst–Pack divisions. Following Testardi [4], Fermi–Dirac broadening is utilized in all calculations, where the amount of broadening is given by equation (1).

3.2. Occurrence of the martensitic transformation

The martensitic transformation is a phenomenon in which the crystal structure spontaneously transforms from cubic to tetragonal upon cooling below the martensitic transformation temperature T_M in low-resistivity Nb_3Sn. This phenomenon was studied in detail by Mailfert *et al* [24], Arko *et al* [25], Watanabe *et al* [26], Axe *et al* [27], and Mentink *et al* [28] in which the effect of the martensitic transformation on the normal state resistivity ρ_n and the phonon properties of low-resistivity Nb_3Sn were investigated. In these analyses, the martensitic transformation temperature T_M was determined at 45 ± 7 K, which corresponds to a normal state resistivity of 27 ± 3 μΩcm [28].

Devantay *et al* [29] and Zhou *et al* [30] performed studies of binary Nb–Sn bulk samples with a variety of tin concentrations. In both investigations the normal state resistivity at T_c, the composition, and the effect of the martensitic transformation on selected x-ray diffraction peaks at room temperature and at 10 K was determined. According to Devantay *et al*, a sample with an average tin concentration of 24.4 at% and a normal state resistivity of 19 μΩcm is a mix of cubic and tetragonal Nb_3Sn at 10 K, while in a sample with a tin concentration of 23.9 at% and a normal state resistivity of 23 μΩcm, no indication of tetragonal distortion was observed. In the investigation by Zhou *et al*, predominantly tetragonal Nb_3Sn was observed in three samples with normal state resistivities below 20.9 μΩcm, while the material was shown to be almost entirely cubic for samples with normal state resistivities above 31.3 μΩcm (not including a sample with an unusually high normal state resistivity, which the

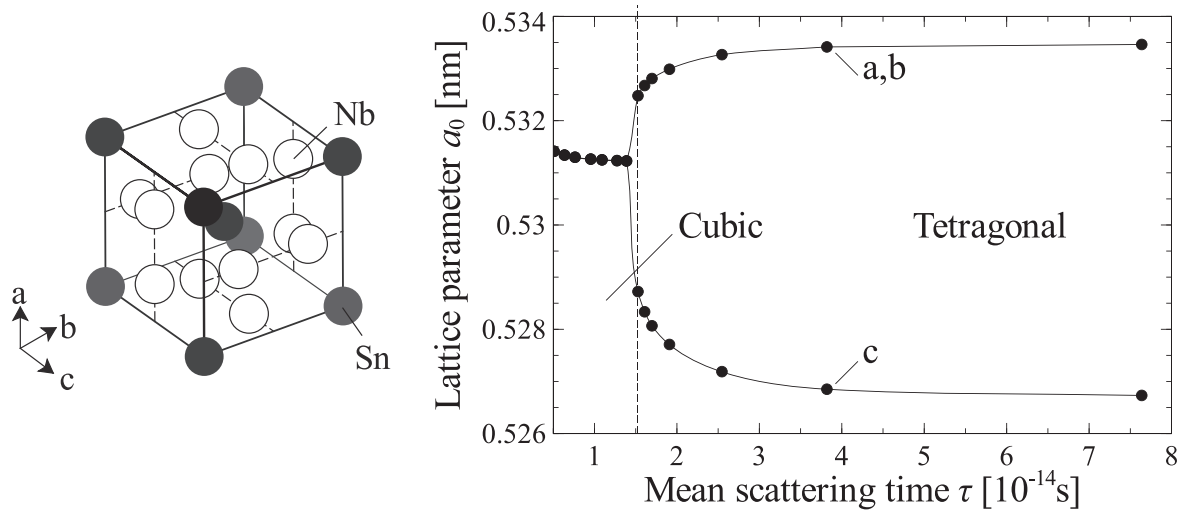

Figure 3. Left: A15 crystal structure of Nb_3Sn. Right: mean scattering time dependent optimal lattice parameters.

author attributed to $NbSn_2$ grain boundary precipitation). In experiments by Goldacker *et al* [31, 32], it was observed that the martensitic transformation in stoichiometric Nb_3Sn could be prevented through various additions including tantalum, titanium, nickel, gallium, and hydrogen. The martensitic transformation was completely suppressed in samples with 0.6 at% H, 2.8 at% Ta, 1.3 at% Ti, and 1 at% Ni, with normal state resistivities of 37 $\mu\Omega$cm, 29 $\mu\Omega$cm, 33 $\mu\Omega$cm, and 30 $\mu\Omega$cm, respectively. The martensitic transformation did, however, occur in a binary bulk sample, also see Guritanu *et al* [33], and a sample with 0.9 at% Ga, with normal states resistivities of 13 and 23 $\mu\Omega$cm. The martensitic transformation temperature range of 20–50 K was observed in a sample with 1.7 at% Ta and a normal state resistivity of 26 $\mu\Omega$cm, and it was concluded that 1.7 at% is very close to the critical tantalum concentration that is required to suppress the martensitic transformation.

In summary, the literature results show that there is a critical value of resistivity (25 $\pm$ 3 $\mu\Omega$cm), above which the material remains cubic (i.e. the martensitic transformation is suppressed) and below which the transformation occurs, independently of whether this resistivity is caused by off-stoichiometry, the presence of ternary impurities, or a non-zero temperature.

The effect of disorder on the optimal crystal structure is investigated here by performing structural optimizations at various values of τ, where τ is indicative of the degree of disorder. The positions of the ions inside the crystal as well as the lattice parameters are optimized simultaneously, under the assumption of no externally applied stress. The structural optimizations start from an orthorhombic configuration and are found to converge to either a cubic or a tetragonal crystal symmetry (see figure 3, right graph). The calculation results indicate that the crystal is preferentially cubic at $\tau < \tau_c$ and tetragonal at $\tau > \tau_c$, and the transition between cubic and tetragonal crystal symmetry is found to occur at a critical mean scattering time τ_c of (1.53 $\pm$ 0.08) $\times$ 10^{-14} s.

Whenever the optimal crystal structure at a given τ is tetragonal, the calculation result additionally indicates sublattice distortion in the niobium chains, a phenomenon that was previously studied from a theoretical perspective by Labbé *et al* [34], from a computational perspective by Sadigh *et al* [35] and Weber *et al* [36], and from an experimental perspective by Shirane *et al* [37]. Conversely, no sublattice distortion is observed whenever the optimal crystal structure is cubic.

Following Testardi *et al* [4], Mattheis *et al* [5, 38], Schachinger *et al* [16], and Allen *et al* [39–41], the normal state resistivity is calculated through an expression which relates ρ_n to $N(E_F)$, v_F, τ, and V, with:

$$\rho_{n,x} = \frac{V}{eN(E_F)v_{F,x}^2\tau}, \tag{18}$$

where $\rho_{n,x}$ is the normal state resistivity in direction x in (Ωm), V the molecular volume (m^3), e is elementary charge in (C), $N(E_F)$ is electron density of states at the Fermi energy in (states $\times$ eV^{-1} $\times$ unit $cell^{-1}$), and $v_{F,x}$ the root mean square Fermi velocity in direction x in (ms^{-1}). According to Schachinger [16], this expression is valid for Nb_3Sn under the assumption that the normal state resistivity is dominated by s-wave scattering of non-magnetic impurities. Following Pickett *et al* [42], the root mean square Fermi velocity is calculated:

$$V = a_x a_y a_z, \tag{19}$$

$$(\hbar v_{F,x})^2 = \frac{\sum_{k,n}(E_x(k,n)^2\delta(E(k,n) - E_F))}{\sum_{k,n}\delta(E(k,n) - E_F)}, \tag{20}$$

$$E_x(k,n) = \frac{E(k + \Delta k_x, n) - E(k,n)}{\Delta k_x}, \tag{21}$$

$$\delta(E) = \frac{1}{2 + \exp\left(\frac{E}{\hbar\tau}\right) + \exp\left(\frac{-E}{\hbar\tau}\right)}, \tag{22}$$

where k is a three-dimensional coordinate in momentum-space in (m^{-1}, m^{-1}, m^{-1}), n the band number, Δk the distance between two k-space coordinates in (m^{-1}), E the energy of electron band n at momentum-space coordinate k in (eV), x a specific direction in momentum space, $\hbar$ the reduced Planck

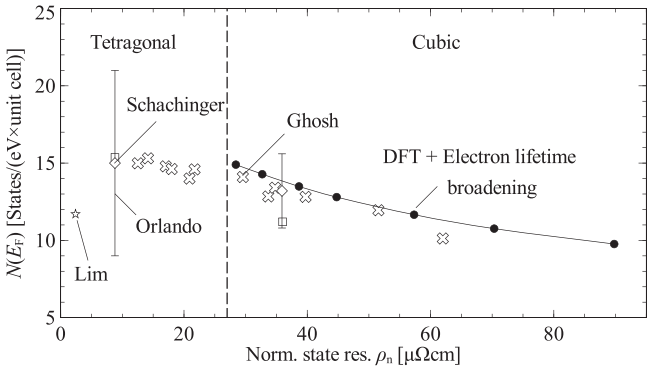

Figure 4. Calculated electron density of states $N(E_F)$ as a function of ρ_n, compared to various literature results from Lim *et al* [43], Schachinger *et al* [16], Orlando *et al* [17], and Ghosh *et al* [18].

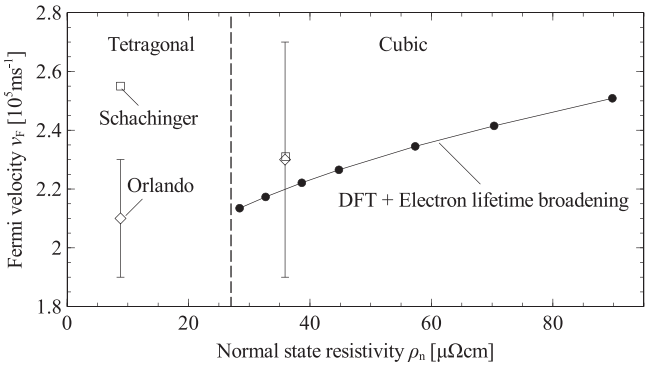

Figure 5. Calculated root mean square Fermi velocity v_F as a function of normal state resistivity ρ_n, compared to literature results after Schachinger *et al* [16] and Orlando *et al* [17].

constant in (eV × s), and $v_{F,x}$ the Fermi velocity along direction x in (ms^{-1}). The total Fermi velocity is related to the directional Fermi velocity through:

$$v_F = \sqrt{v_{F,a}^2 + v_{F,b}^2 + v_{F,c}^2}, \tag{23}$$

where a, b, and c represent the three orthogonal crystal directions (figure 3, left graph).

In this manner, the electron density of states, the Fermi velocity, and the lattice parameters at $\tau = (1.53 \pm 0.08) \times 10^{-14}$ s are calculated with $N(E_F) = 15.13 \pm 0.23$ states/(eV × unit cell), $v_{F,x} = (1.225 \pm 0.008) \times 10^5$ ms^{-1}, $v_F = (2.121 \pm 0.014) \times 10^5$ ms^{-1}, and $a_x = a_y = a_z = 0.5312$ nm. Using equation (18), the critical normal state resistivity ρ_c is calculated at 27.0 ± 1.4 μΩcm, where Nb_3Sn is preferentially cubic when $\rho_n > \rho_c$ and preferentially tetragonal when $\rho_n < \rho_c$.

The calculated ρ_c of 27.0 ± 1.4 μΩcm is consistent with the critical resistivity 25 ± 3 μΩcm that is derived from experimental observations, which is an indication of the applicability of the electron lifetime broadening hypothesis (section 2.1).

3.3. Comparison of calculated N (E_F), v_F, and phonon dispersion curves to literature results

The normal state resistivity dependent electron density of states $N(E_F)$ and Fermi velocity v_F were previously derived from experimental data by by Lim *et al* [43], Schachinger *et al* [16], Orlando *et al* [17], and Ghosh *et al* [18]. The analyses of Schachinger *et al* and Orlando *et al* were performed on two samples with different Sn contents, while the analysis of Ghosh *et al* was performed on stoichiometric Nb_3Sn in which disorder was introduced through radiation damage. These analyses utilized various experimental observations, including the heat capacity, the critical temperature, and the upper critical field.

Ab initio calculations of the normal state resistivity dependent electron density of states and Fermi velocity are performed and compared to literature results. The results are found to be consistent for both the electron density of states (figure 4) and the Fermi velocity (figure 5). The calculations were only performed in the preferentially cubic regime (also see section 3.2). Performing calculations on a single unit cell in the preferentially tetragonal regime gives incorrect results, because this implicitly and incorrectly assumes that the *c*-axis is perfectly aligned throughout the crystal. In reality, it was argued by Kartha *et al* [44] and experimentally demonstrated by Goringe *et al* [45] and Onozuka *et al* [46] in the case of V_3Si, that the martensitic transformation results in tweed modulation. This phenomenon describes the division of the sample into different regions, where the orientation of the short *c*-axis (figure 3, right graph) varies between the regions. Very fine tweed patterns are observed, with widths as fine as 10 nm [45], i.e. only one order of magnitude above the lattice constant of the material (see figure 3, right graph). It is not understood how the formation of the tweed pattern affects the electronic properties nor the local stress and strain state. While this phenomenon might be incorporated in the DFT calculations through the use of a very large supercell, the computational requirements of such a calculation are extreme. This is why the calculations in this paper only consider the properties of preferentially cubic Nb_3Sn.

In figure 6, calculated phonon dispersion curves are compared to the experimental observations by Axe *et al* [47], and Pintschovius *et al* [48], while the phonon density of states at three different degrees of disorder is compared to an experimental observation of the frequency dependent phonon density of states, after Schweiss *et al* [13] (figure 7). This comparison is somewhat imperfect, as it compares calculation results of cubic and thus higher-resistivity Nb_3Sn to experimental results of low-resistivity Nb_3Sn.

In an in-depth discussion of inelastic neutron scattering measurements, Axe *et al* [27] identify two mechanisms that contribute to a broadening of the phonon density of states, which are phonon scattering off of thermally excited quasi-particles and direct excitation of quasi-particles across the superconducting gap by phonons. These two phenomena contribute to a broadening with a full width half max (FWHM) of 1.2 meV. To allow for a qualitative comparison of the calculation results and the experimental observations, the calculation results are convoluted with a gaussian function with an FWHM of 1.2 meV (figure 7). This does not affect the derived electron–phonon constant and the characteristic frequency, as these are integrals over the entire frequency range.

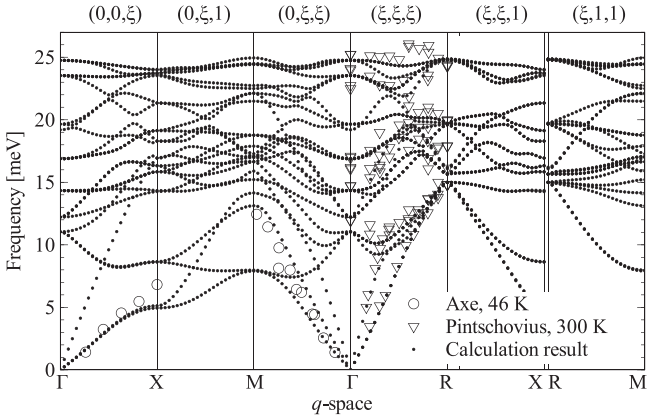

Figure 6. Calculated phonon dispersion curves of disordered Nb_3Sn, compared to experimental observations. The phonon dispersion curves are calculated at $\tau = 0.76 \times 10^{-15}$ s, which corresponds to a normal state resistivity of 57.3 $\mu\Omega$cm. The calculation result is compared to experimental observations by Pintschovious *et al* [48] and Axe *et al* [47].

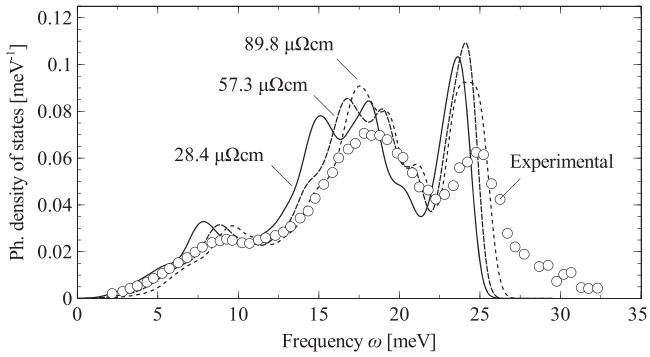

Figure 7. Calculated phonon density of states $F(\omega)$ as a function of vibrational frequency ω, compared to experimental observations. The phonon densities of states are calculated at $\tau = 1.45 \times 10^{-15}$ s, 0.76×10^{-15} s, and 0.51×10^{-15} s, which corresponds to 28.4, 57.3, and 89.8 $\mu\Omega$cm respectively. The experimental result is of low-resistivity Nb_3Sn, after Schweiss *et al* [13].

Apart from these details, the calculation results are generally very similar to the experimental observations (figures 6 and 7). In general, the calculated frequencies of the various vibrational modes are somewhat low in comparison to the experimental observations, although it is not clear whether this is a small systematic error in the calculation result or due to the imperfect nature of the comparison discussed here.

3.4. Calculated versus experimentally observed Eliashberg spectra of high-resistivity Nb_3Sn

To validate whether ω_0 and $\alpha^2_{\mathrm{IM,eff}}$ are indeed weakly dependent or independent of disorder and thus may be considered as global constants (section 2.2), $\alpha^2(\omega)F(\omega)$ of high-resistivity Nb_3Sn is determined from the calculated electron and phonon density of states through equation (15) and compared to experimental observations of stoichiometric and off-stoichiometric Nb–Sn tunnel junctions by Rudman *et al* [8] (figure 8). Consistent with Rudman's observations, the calculation result indicates that three peaks are present and

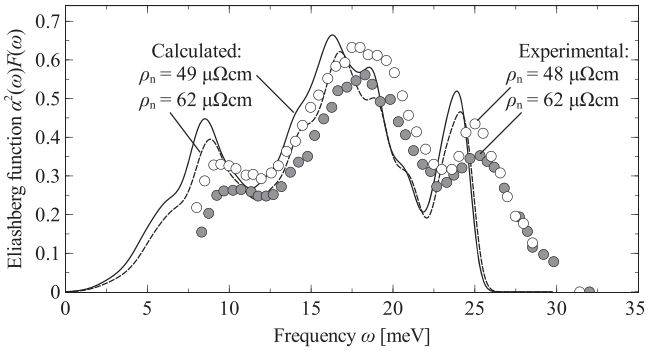

Figure 8. Calculated Eliashberg function $\alpha^2(\omega)F(\omega)$ as a function of ω of disordered Nb_3Sn, compared to $\alpha^2(\omega)F(\omega)$ derived from off-stoichiometric tunnel junctions, after Rudman *et al* [8].

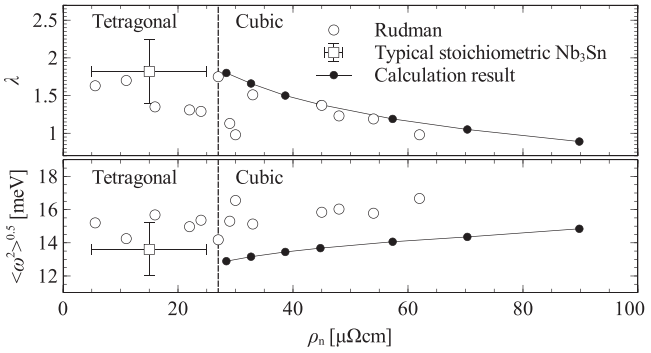

Figure 9. Calculated electron–phonon coupling constant λ and characteristic phonon frequency $\langle\omega^2\rangle^{0.5}$ as a function of normal state resistivity ρ_n, compared to values derived from experimental observations by Rudman *et al* [8]. Also shown are the average literature values and standard deviations of low-resistivity Nb_3Sn, shown in table 1.

that the amplitude of $\alpha^2(\omega)F(\omega)$ decreases with increasing amount of disorder (i.e. increasing ρ_n). The frequencies of the peaks in the calculated spectra are somewhat low frequency in comparison to the experimental result, which could mean that a small systematic error is present in the phonon density of states calculation. However, Rudman *et al* [8] points out that some anomalies were observed in the tunnel junction data, which might also imply a slight systematic upward bias in the experimental results.

From the calculated Eliashberg spectra, λ and $\langle\omega^2\rangle^{0.5}$ are derived through equations (2) and (6) and compared to experimental observations by Rudman *et al* [8] (figure 9). In addition, from the Eliashberg spectra published by various authors (figure 1, left graph), λ and $\langle\omega^2\rangle^{0.5}$ are derived using equations (2) and (6) (table 1). The calculated values of λ are very close to Rudman's observations, while the calculated $\langle\omega^2\rangle^{0.5}$ is somewhat lower than Rudman's values over the entire ρ_n range, albeit within one standard deviation of the mean literature values (table 1).

In summary, the calculated electron–phonon coupling constant λ is consistent with experimental results over the investigated disorder range. The characteristic frequency $\langle\omega^2\rangle^{0.5}$ is somewhat below the experimentally observed number, but the general trend is consistent. This result

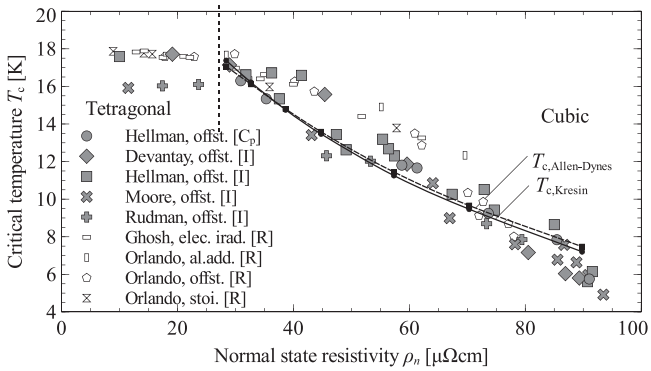

Figure 10. Calculated critical temperature T_c as a function of normal state resistivity ρ_n, compared to experimental literature data.

indicates that, within the uncertainty of this comparison, it seems reasonable to treat $\alpha^2_{IM,eff}$ and ω_0 as global constants, which supports assumption #2 (section 2.2).

4. Comparison of calculation results and experimental observations on the superconducting phase boundary

4.1. Critical temperature T_c as a function of normal state resistivity

Using the expressions for critical temperature given by Kresin (equation (16)) and Allen–Dynes (equation (17)), the normal state resistivity dependent critical temperature is calculated and compared to experimental results (figure 10).

In this comparison, the emphasis is placed on inductive and heat capacity measurements instead of resistivity measurements. While it is relatively straightforward to produce samples of Nb_3Sn with very sharp T_c transitions at $T_c \approx 18$ K, producing low-T_c Nb–Sn samples with sharp T_c transitions is a major challenge. Investigations of the T_c width in low-T_c samples indicate that the T_c transitions are typically several Kelvin wide (see Hellman *et al* [49] and Mentink *et al* [50]). In resistivity measurements, the measured normal state resistivity may be considered an effective average, but only a fraction of the sample needs to be superconducting in order to form a superconducting path and short the sample. This means that an upward bias in a direct T_c versus ρ_n measurement is unavoidable. Inductive and heat capacity measurements do not suffer from this problem so that the latter in particular is considered a 'true' bulk measurement. Unfortunately, the normal state resistivity of samples investigated through inductive and heat capacity measurements is not always known. However, the relationship between normal state resistivity and composition in binary Nb–Sn samples where disorder is not introduced through some other fashion is well understood (Godeke [51], Flükiger [52]), and was empirically summarized by Godeke *et al* [51], with:

$$\rho_n(\beta) = 91(1 - (7\beta - 0.75)^4) + 3.4 \quad \text{for } \beta \leqslant 25\%, \quad (24)$$

where β is the atomic tin fraction, and ρ_n is the residual resistivity (i.e. the normal state resistivity slightly above T_c) in ($\mu\Omega$cm). The uncertainty in this description is estimated to be about 5 $\mu\Omega$cm. Thus, in measurements where the off-stoichiometric composition rather than the normal state resistivity is known, the normal state resistivity is calculated through equation (24).

Besides the resistivity measurements of Orlando *et al* [17], in which disorder is introduced through anti-site disorder, aluminum additions, and off-stoichiometry (indicated as 'stoi.', 'al.add', and 'offst.' respectively in figure 10), and the resistivity measurements of Ghosh *et al* [18] in which disorder is introduced through electron irradiation (indicated as 'elec. irad' in figure 10), various heat capacity and inductive measurements of off-stoichiometric Nb–Sn samples are shown, after Hellman *et al*, Devantay *et al* [29], Moore *et al* [53], and Rudman *et al* [54].

The comparison between the calculation results and experimental observations shows a high degree of consistency, in particular with regards to induce and heat capacity measurements.

4.2. Upper critical magnetic field H_{c2} as a function of critical temperature T_c

In addition to the critical temperature, the upper critical field is investigated. The upper critical magnetic field in phonon-mediated superconductors has been thoroughly investigated in the past, resulting in a number of descriptions. After the initial success of the Ginzburg–Landau–Abrikosov–Gor'kov (GLAG) theory [55–57], various corrections were considered and developed to account for the different phenomena which affect the upper critical magnetic field. The temperature dependence of H_{c2} was described by Maki and De Gennes [58], under the assumption of a dirty superconductor, a spherical Fermi surface, a weakly energy dependent electronic density of states, and a weak-coupling interaction. Subsequent refinements were made to include various effects, such as the impurity dependence of H_{c2} by Helfand *et al* [59, 60], Fermi surface anisotropy by Hohenberg *et al* [61] and Schachinger *et al* [16], spin–orbit coupling by Werthamer *et al* [62], Schopohl *et al* [63], and Rieck *et al* [64], anisotropic scattering by Schopohl *et al* [65], Pauli paramagnetic limiting by Orlando *et al* [17, 66] and Rieck *et al* [64], strong coupling effects by Werthamer *et al* [67], Masharov [68], and Schossmann *et al* [69], *p*- and *d*-wave scattering by Rieck *et al* [64] and the energy-dependence of N (E_F) by Schossmann *et al* [70]. A useful overview of these various mechanisms is provided by Rieck *et al* [64].

A number of authors investigated the temperature dependence of the upper critical magnetic field, in an attempt to determine which of the aforementioned phenomena should be considered to get a realistic description of Nb_3Sn. Orlando *et al* [17] considered the influence of Pauli paramagnetic limiting and spin–orbit coupling and found that a large amount of spin–orbit coupling was required to counteract the reduction of $H_{c2}(0)$ due to Pauli paramagnetic limiting. However, in a subsequent paper by the same authors [66], it was pointed out that the original paper incorrectly assumed a

first-order transition rather than a second-order transition, resulting in an incorrect description of the Pauli limiting field. Schachinger *et al* [16] used a description which emphasized Pauli paramagnetic limiting and Fermi surface anisotropy, without considering spin–orbit coupling, and investigated the same experimental data that was obtained by Orlando *et al* [17]. In this approach, a free parameter was used to describe the extent by which Fermi anisotropy raises $H_{c2}(0)$.

Rieck *et al* constructed a highly comprehensive model that takes into account various phenomena, such as Fermi surface anisotropy, Pauli limiting, *s*-, *p*- and *d*-wave scattering, and spin–orbit coupling where the magnitude of each of these phenomena is described with a free parameter. In evaluating the same experimental data that Orlando *et al* [17] obtained, Rieck *et al* determined that the experimental data was accurately described with dirty limit theory in the case of the off-stoichiometric sample and clean limit theory in the case of the low-resistivity stoichiometric sample, and that allowing for fitting of the various free parameters which account for the influence of the other physical phenomena only led to a minor improvement in fitting accuracy. In other words, the influence of the various phenomena is minor or the influences of the various phenomena cancel each other out.

Consistent with this analysis, it was subsequently demonstrated by Godeke *et al* [71] that the Maki–De Gennes description (which is a dirty limit, weak coupling approximation that does not consider other phenomena such as Pauli limiting and spin–orbit coupling) matches the observed temperature dependence of H_{c2} in a large variety of binary and ternary Nb_3Sn wires, bulk samples, and thin films.

It should be emphasized that most of these analyses mainly concern themselves with the experimentally determined temperature-dependent upper critical field. Here, however, H_{c2} at 0 K is calculated from other microscopic parameters such as the calculated Fermi velocity.

Figure 11 shows a collection of experimental observations of $H_{c2}(0)$ as a function of T_c in binary and ternary Nb_3Sn samples. Unlike the $T_c(\rho_n)$ dependence (figure 10), where the use of resistively determined T_c as a function of ρ_n measurements can lead to incorrect results, resistance measurements can be used to determine the $H_{c2}(0)$ as a function of T_c relationship, because in the preferentially cubic regime, $\mu_0 H_{c2}(0)$ rises with increasing T_c and thus a resistive measurement of $H_{c2}(T)$ probes the same compositional fraction inside a sample as a resistive measurement of T_c.

The experimental observations (figure 11) consist of resistive measurements of thin films, bulk samples, and strands, after Mentink *et al* [50, 72], Zhou *et al* [30], Jewell *et al* [73], Orlando *et al* [2], Devantay *et al* [29], and Godeke *et al* [71]. In addition, radio-frequency measurements of bulk material were taken by Foner *et al* [74], and magnetic measurements of bulk material were taken by Arko *et al* [25] and Jewell *et al* [73]. Critical current density measurements of binary thin film samples were performed by Mentink *et al* [3]. Magnetic measurements of Nb_3Sn wires were taken by Naus *et al* [75], in which T_c and the Kramer extrapolated $H_K(4.2\,K)$ were determined. From these measurements,

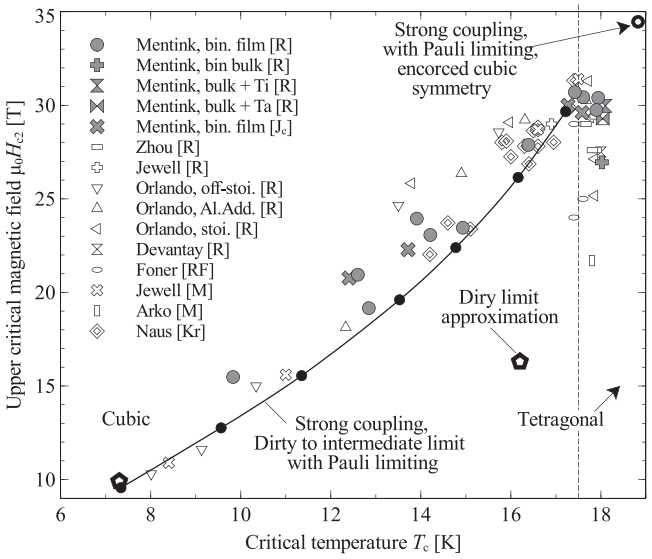

Figure 11. Calculated upper critical field $\mu_0 H_{c2}(0)$ as a function of critical temperature T_c, compared to literature data.

$H_{c2}(0)$ was extrapolated through a method that is discussed elsewhere [50].

Here, the upper critical field is calculated in the dirty to intermediate limit, where strong-coupling corrections and Pauli limiting are accounted for. The influence of these phenomena is chosen because they are well-described in literature and do not require the use of free parameters. The accuracy of the calculations may potentially be enhanced further, which is discussed in section 5.

The slope of $\delta H_{c2}^{+}/\delta T$ at 0 T is described by GLAG theory [5, 17, 55–57], with:

$$\frac{-\delta(\mu_0 H_{c2})}{\delta T}\Big|_{T_c} = \left(\frac{24\pi^2 k_B^2}{7\zeta(3)\hbar e}\right)\frac{\eta_{H_{c2}} T_c (1+\lambda)^2}{v_F^2 X(Z)}, \qquad (25)$$

where $\delta(\mu_0 H_{c2})/\delta T$ is in (T K^{-1}), $\zeta(3)$ is Apery's constant. η_{Hc2} is the strong coupling correction factor for $\mu_0 H_{c2}$ [68]. Z is the reduced collision frequency [59], which is closely related to mean scattering time:

$$Z = \frac{\hbar}{2\pi k_B T_c (1+\lambda)\tau} = \frac{\hbar v_F}{2\pi k_B T_c (1+\lambda) l_{mfp}}. \qquad (26)$$

Here l_{mfp} is the mean free path. $X(Z)$ is the Gor'kov function [57], with:

$$X(Z) = \frac{\sum_{v=0}^{\infty}(2v+1)^{-2}(2v+1+Z)^{-1}}{\sum_{v=0}^{\infty}(2v+1)^{-3}}. \qquad (27)$$

The upper critical field H_{c2}^{+} is calculated from $\delta(H_{c2})/\delta T$ using parameter h_{c2}^{*}, with:

$$H_{c2}^{+}(0) = h_{c2}^{*}(Z)\frac{-\delta(H_{c2})}{\delta T}\Big|_{T_c} T, \qquad (28)$$

Combining equations (25) and (28), the upper critical

magnetic field without Pauli limiting H_{c2}^{+} is expressed as:

$$\mu_0 H_{c2}^{+}(0) = \eta_{Hc2} X(Z)^{-1} h_{c2}^{*}(Z) \left(\frac{24\pi^2 k_B^2}{7\zeta(3)\hbar e} \right) \frac{T_c^2 (1+\lambda)^2}{v_F^2}. \tag{29}$$

According to Masharov *et al* [68] the strong coupling correction factor η_{Hc2} is expressed as:

$$\eta_{H_{c2}} = 1 + \left(\frac{\pi k_B T_c}{\langle \omega^2 \rangle^{0.5}} \right) \left(0.6 \ln \left(\frac{\langle \omega^2 \rangle^{0.5}}{k_B T_c} \right) - 0.26 \right), \tag{30}$$

where $k_B T_c$ is in (eV), $\langle \omega^2 \rangle^{0.5}$ is in (eV), and η_{Hc2} is a dimensionless parameter. At $T_c = 17.2$ K (i.e. $\rho_n = 28.4$ $\mu\Omega$cm), η_{Hc2} is calculated at 1.13, while at $T_c = 7.3$ K (i.e. $\rho_n = 90$ $\mu\Omega$cm), it is calculated at 1.03. The Z dependent h_{c2}^{*} is taken from Rieck *et al* [64]. This function is equal to the dirty limit value of 0.69267 over most of the disorder range, but it rises to 0.72 near the clean limit. The Z dependent X is calculated through equation (27). The result is linearized between $Z = 1.56$ to $Z = 17.5$:

$$X(Z)^{-1} h_{c2}^{*}(Z) \approx 0.608Z + 0.766, \tag{31}$$

which results in an average deviation of 0.4% and a maximum deviation of 0.6% between the exact and linearized expressions in the range of $Z = 1.56$–17.5. $H_{c2}^{+}(0)$ is then expressed as:

$$\mu_0 H_{c2}^{+}(0) = \eta_{Hc2} \left(C_{O1} \frac{T_c^2 (1+\lambda)^2}{v_F^2} + C_{O2} \frac{T_c (1+\lambda)}{v_F l_{mfp}} \right), \tag{32}$$

$$C_{O1} = \frac{0.766 \times 24\pi^2 k_B^2}{7\zeta(3)\hbar e} = 2.43 \times 10^8 \ (\mathrm{Tm^2\,K^{-2}\,s^{-2}}), \tag{33}$$

$$C_{O2} = \frac{0.608 \times 12\pi k_B}{7\zeta(3) e} = 2.35 \times 10^{-4} \ (\mathrm{Tm^2\,K^{-1}\,s^{-1}}). \tag{34}$$

After Orlando *et al* [66], the Pauli paramagnetic limiting field in the absence of spin–orbit coupling is expressed as:

$$\mu_0 H_P(0) = 1.858 \times T_c (1+\lambda), \tag{35}$$

where T_c is in (K) and $\mu_0 H_P$ is in (T). Following Orlando *et al* [66], the expression for $H_{c2}(0)$ is:

$$(H_{c2}(0))^{-2} = (H_{c2}^{+}(0))^{-2} + 2(H_P(0))^{-2}. \tag{36}$$

Relative to the $H_{c2}^{+}(0)$, Pauli limiting reduces $H_{c2}(0)$ by 13% at $T_c = 17.2$ K (i.e. $\rho_n = 28.4$ $\mu\Omega$cm), and 17% at $T_c = 7.3$ K (i.e. $\rho_n = 90$ $\mu\Omega$cm).

The final result is shown in figure 11. It is clear that the calculated results are generally consistent with experimental observations, albeit somewhat on the low end of the experimental range, in particular in the T_c regime of 14–16 K.

4.3. Effect of the martensitic transformation on T_c and $\mu_0 H_{c2}(0)$

In figure 11 a significant drop in $\mu_0 H_{c2}(0)$ is observed near $T_c = 18$ K, that seems to correlate with the onset of the tetragonal regime. Here we argue that these two phenomena are related.

To investigate this possibility, a calculation is performed where the martensitic transformation is suppressed, i.e. rather than allowing the unit cell to find the optimal (non-cubic) configuration, cubic symmetry is enforced and the properties of the crystal are evaluated. Unfortunately, only the electronic properties of this unstable crystal can be evaluated, as the unstable nature prevents calculation of the vibrational properties. Instead, the phonon density of states at $\tau = 1.45 \times 10^{-14}$ s, corresponding to $\rho_n = 26.7$ $\mu\Omega$cm, is taken. At $\tau = 1.91 \times 10^{-14}$ s, corresponding to $\rho_n = 21.4$ $\mu\Omega$cm, a critical temperature of 18.8 K and an upper critical field of 34.5 T is found, thus implying that if the tetragonal transformation does not occur, the superconducting properties continue to rise with decreasing normal state resistivity.

This statement is controversial and in past publications two arguments were given for to explain why the occurrence of the martensitic transformation does not result in the reduction of $\mu_0 H_{c2}$:

First of all, it is commonly assumed that Nb_3Sn may be approximated as a dirty limit superconductor. This means that in equation (26), Z may be approximated at ∞ and $X(Z)$ may be approximated at $0.853 \times Z$. Also ignored strong coupling effects and Pauli limiting, the upper critical field may then be related to the electronic heat capacity, so that a rather simple expression of $\mu_0 H_{c2}(0)$ may be deduced:

$$\gamma^{*} = \frac{\pi^2 k_B^2 N(E_F)(1+\lambda)}{3e}, \tag{37}$$

$$\mu_0 H_{c2,\mathrm{dirty}}(0) = C_{\mathrm{dirty}} T_c \gamma^{*} \rho_n, \tag{38}$$

$$C_{\mathrm{dirty}} = 3.11 \times 10^3 \ [\mathrm{TKm^2J^{-1}\Omega^{-1}}]. \tag{39}$$

where γ^{*} is the renormalized electronic heat capacity in (J $K^{-2}m^{-3}$) (see, for instance, analyses by Orlando *et al* [17] and Guritanu *et al* [33]). Thus, if this equation is applicable towards the clean limit, then $\mu_0 H_{c2}(0)$ is proportional to the normal state resistivity, so that one may speculate that the drop in $\mu_0 H_{c2}(0)$ is due to the drop in ρ_n. A problem with this expression is that Nb_3Sn is a intrinsic type II superconductor, which means that it exhibits type-II behavior without being in the dirty limit (see for instance Fetter and Hohenberg [76]). Indeed, while the calculation result matches the experimental in the dirty limit (at $T_c = 7.2$ K), $\mu_0 H_{c2}(0) = 16.2$ T is found at $T_c = 16.2$ K which is highly inconsistent with the experimental data (figure 11). Given the inapplicability of equation (37) towards the clean limit, as well as the fact that $\mu_0 H_{c2}(0)$ is no longer proportional to ρ_n when the material is not in the dirty limit, this argument appears to be incorrect.

A more recent argument is given by Zhou *et al* [30], in which a detailed experimental investigation was undertaken to show that Nb–Sn samples may contain tetragonal Nb_3Sn while simultaneously having an upper critical field of 29 T, as determined by resistive measurements. However, after a subsequent thorough investigation which considered the possibility of minor compositional inhomogeneity in the samples, it was concluded that the observed $\mu_0 H_{c2}(0)$ of 29 T is likely due to a small fraction of cubic Nb–Sn in the

samples, and that the drop in $\mu_0 H_{c2}(0)$ does coincide with the occurrence of tetragonal Nb_3Sn [77].

5. Discussion

One of the starting assumptions taken in this paper is that disorder is a major determinant for the occurrence of the martensitic transformation, T_c and $H_{c2}(0)$, regardless whether disorder is introduced through anti-site disorder, radiation damage, or off-stoichiometry, as was previously argued by Orlando *et al* [2]. The consistency between the various calculation results and experimental observations is a strong indication that this assumption is indeed reasonable.

One could further speculate that disorder uniquely determines the microscopic properties (i.e. $N(E_F)$, v_F, $F(\omega)$, l_{mfp}) of Nb_3Sn, regardless of the manner in which disorder is introduced. The validity of this statement was investigated by performing supercell calculations at various niobium to tin ratios for a given τ. The results of this investigation indicate that the presence of excess niobium results in a reduced $N(E_F)$ even when τ is fixed. For instance, fixing τ at 1.27×10^{-14} s and comparing supercells with 25, 23.4 and 21.9 at% Sn, $N(E_F) = 14.1$, 11.2, and 9.7 states/(eV $\times$ unit cell) are found, respectively. Thus, when off-stoichiometry is considered, τ does not uniquely determine the microscopic properties and electron-lifetime broadening should be considered a rather poor proxy for off-stoichiometry. The strong link between ρ_n, T_c and $\mu_0 H_{c2}(0)$ as observed by Orlando *et al* [2] may be attributed to the fact that ρ_n is inversely proportional to $N(E_F)$, T_c is roughly proportional to λ and thus to $N(E_F)$, and $\mu_0 H_{c2}(0)$ is strongly determined by T_c. Noting that T_c versus ρ_n is roughly inversely proportional to ρ_n (figure 10) it is clear that a reduction in $N(E_F)$ due to off-stoichiometry leads to a similar T_c versus ρ_n dependency as a reduction in $N(E_F)$ resulting from an increase in τ. In summary, introducing an electron-lifetime broadening assumption to investigate disorder is a reasonable approach for investigating the influence of disorder in general, but further research is needed to distinguish between different types of disorder, for instance anti-site disorder and off-stoichiometry.

In this paper, the effective Coulomb repulsion term is treated as a constant equal to 0.125. This statement is based on experimental evidence, for instance the experimentally observations of μ^* by Rudman in a series of Nb_3Sn samples over a wide disorder range (figure 2). In the paper by Bennemann and Garland [78] two different estimates are provided for transition metals, yielding 0.2 and 0.17 for Nb_3Sn with a critical temperature of 18 K. Conversely, in other papers the coupling constant is commonly held at about 0.1 for Nb_3Sn over a wide disorder range [17, 19, 20]. Given this uncertainty in the literature and the availability of experimental data by Rudman (figure 2), the constant μ^* used here seems reasonable. To illustrate, an uncertainty in μ^* of 0.02 corresponds to a T_c uncertainty of about 1 K over the entire disorder range.

The calculated $\mu_0 H_{c2}(0)$ versus T_c curve in figure 11 is generally consistent with the experimental data within the scatter of the experimental data. Previous published investigations and reviews identify a host of potential phenomena that may impact $\mu_0 H_{c2}(0)$ (see section 4.2). For instance, for a given T_c, $\mu_0 H_{c2}(0)$ may be further increased due to Fermi surface anisotropy as described by Schachinger *et al* [16], leading to a reported 5% increase (i.e. another 1.3 T) in $\mu_0 H_{c2}(0)$ at T_c =16 K. It is clear from figure 11 that incorporating this phenomenon would indeed result in greater overlap between the experimental and calculated $\mu_0 H_{c2}(0)$. A downside of Schachinger's description and other similar descriptions is that it does not directly relate the degree of increase in $\mu_0 H_{c2}(0)$ to properties of the Fermi surface but rather relies on free parameters. This is undesirable as it affects the reliability of the calculations, and as such, a less accurate description of the upper critical field is used here.

6. Conclusions

A detailed investigation is performed to investigate the effects of disorder on the normal state and superconducting properties of Nb_3Sn. This investigation combines first-principles calculations with microscopic theory. A comprehensive literature review is performed to accomplish this goal.

Evaluated properties include the occurrence of the martensitic transformation, the electron density of states, the Fermi velocity, the phonon density of states, the Eliashberg spectrum, the critical temperature, and the upper critical magnetic field as a function of disorder. This investigation provides a comprehensive review of how Nb_3Sn may be understood in terms of microscopic theory.

The calculation results are validated through comparisons to experimental observations as well as previously published calculation results. An excellent degree of consistency is demonstrated.

Acknowledgments

This work was supported in part by the Director, Office of Science, High Energy Physics, Basic Energy Sciences, the US Department of Energy under Contract DE-AC02-05CH11231 (FH supported by NEMM program at LBNL). The DFT and DFPT calculations were performed using computing resources from the Cornell NanoScale Science and Technology Facility and the National Energy Research Scientific Computing Center, with special thanks to Derek Stewart and Robert Ryne. Also thanks to Cissy for the spelling and grammar checks.

References

[1] Matthias B T, Geballe T H, Geller S and Corenzwit E 1954 Superconductivity of Nb_3Sn *Phys. Rev.* **95** 1435

[2] Orlando T P, Alexander J A, Bending S J, Kwo J, Poon S J, Hammond R H, Beasley M R, McNiff E J and Foner S 1981 The role of disorder in maximizing the upper critical field in the Nb–Sn system *IEEE Trans. Magn.* **17** 368–9

[3] Mentink M G T 2014 An experimental and computation study of strain sensitivity in superconducting Nb_3Sn *PhD Thesis* University of Twente

[4] Testardi L R and Mattheiss L F 1978 Electron lifetime effects on properties of A15 and bcc materials *Phys. Rev. Lett.* **41** 1612–5

[5] Mattheiss L F and Testardi L R 1979 Electron-lifetime effects on properties of Nb_3Sn, Nb_3Ge, and Ti–V–Cr alloys *Phys. Rev.* B **20** 2196–200

[6] Eliashberg G M 1960 *Zh. Eksp. Teor. Fiz.* **38** 966

[7] Markiewicz W D 2004 Elastic stiffness model for the critical temperature T_c of Nb_3Sn including strain dependence *Cryogenics* **44** 767–82

[8] Rudman D A and Beasley M R 1984 Microscopic superconducting parameters from tunneling in A15 Nb–Sn *Phys. Rev.* B **30** 2590–4

[9] Shen L Y L 1972 Tunneling into a high-T_c superconductor-Nb_3Sn *Phys. Rev. Lett.* **29** 1082–6

[10] Geerk J, Kaufmann U, Bangert W and Rietschel H 1986 Electron tunneling into Nb_3Sn, Nb_3Ge, and Nb_3Al *Phys. Rev.* B **33** 1621–6

[11] Freericks J K, Liu A Y and Quandt A 2002 Nonconstant electronic density of states tunneling inversion of A15 superconductors: Nb_3Sn *Phys. Rev.* B **64** 224510

[12] Wolf E L 1978 Electron tunneling spectroscopy *Rep. Prog. Phys.* **41** 1439–508

[13] Schweiss B P, Renker B, Schneider E and Reichardt W 1976 Phonon spectra of A-15 compounds and ternary molybdenum chalcogenides *Superconductivity in d- and f-Band Metals* (New York: Plenum Press) pp 189–208

[14] McMillan W L 1968 Transition temperature of strong-coupled superconductors *Phys. Rev.* **167** 331–44

[15] Hopfield J J 1969 Angular momentum and transition-metal superconductivity *Phys. Rev.* **186** 443–51

[16] Schachinger E and Prohammer M 1988 Anisotropy effects in the A-15 superconductor Nb_3Sn *Physica* C **156** 701–6

[17] Orlando T P, McNiff E J Jr, Foner S and Beasley M R 1979 Critical fields, Pauli paramagnetic limiting, and material parameters of Nb_3Sn and V_3 Si *Phys. Rev.* B **19** 4545–61

[18] Ghosh A K, Gurvich M, Wiesmann H and Strongin M 1978 Density of states in two A-15 materials *Phys. Rev.* B **18** 6116–21

[19] Kresin V Z 1987 On the critical temperature for any strength of the electron–phonon coupling *Phys. Lett.* A **122** 434–8

[20] Allen P B and Dynes R C 1975 Transition temperature of strong-coupled superconductors reanalyzed *Phys. Rev.* B **12** 905–22

[21] Giannozzi P *et al* 2009 Quantum espresso: a modular and open-source software project for quantum simulations of materials *J. Phys.: Condens. Matter* **21** 395502

[22] Perdew J P, Chevary J A, Vosko S H, Jackson K A, Pederson M R, Singh D J and Fiolhais C 1992 Atoms, molecules, solids, and surfaces: applications of the generalized gradient approximation for exchange and correlation *Phys. Rev.* B **46** 6671–87

[23] Quantum Espresso website: http://quantum-espresso.org/

[24] Mailfert R, Batterman B W and Hanak J J 1967 Low temperature structure transformation in Nb_3Sn *Phys. Lett.* **24A** 315–6

[25] Arko A J, Lowndes D H, Muller F A, Roeland L W, Wolfrat J, van Kessel A T, Myron H W, Mueller F M and Webb G W 1978 De Haas–van Alphen effect in the high-T_c A15 superconductors Nb_3Sn and V_3Si *Phys. Rev. Lett.* **40** 1590–3

[26] Watanabe Y, Toyota N, Inoue T, Komatsu H and Iwasaki H 1988 An x-ray diffraction study of martensitic transformation in Ti-Doped Nb_3Sn *Japan. J. Appl. Phys.* **27** 2218–23

[27] Axe J D and Shirane G 1973 Inelastic-neutron-scattering study of acoustic phonons in Nb_3Sn *Phys. Rev.* B **8** 1965–77

[28] Mentink M G T, Dhalle M M J, Dietderich D R, Godeke A, Goldacker W, Hellman F and ten Kate H H J 2012 Towards analysis of the electron density of states of Nb_3Sn as a function of strain *AIP Conf. Proc.* **1435** 225–32

[29] Devantay H, Jorda J L, Decroux M and Muller J 1981 The physical and structural properties of superconducting A15-type Nb–Sn alloys *J. Mat. Soc.* **16** 2145–54

[30] Zhou J, Jo Y, Sung Z H, Zhou H, Lee P J and Larbalestier D C 2011 Evidence that the upper critical field of Nb_3Sn is independent of whether it is cubic or tetragonal *Appl. Phys. Lett.* **99** 122507

[31] Goldacker W and Flükiger R 1985 Phase transitions and superconducting properties of binary and Ti, Ta, Ga and H alloyed Nb_3Sn *Physica* B **135** 359–63

[32] Flükiger R, Senatore C, Cesaretti M, Buta F, Uglietti D and Seeber B 2008 Optimization of Nb_3Sn and MgB_2 wires *Supercond. Sci. Technol.* **21** 054015

[33] Guritanu V, Goldacker W, Bouquet F, Wang Y, Lortz R, Goll G and Junod A 2004 Specific heat of Nb_3Sn: the case for a second energy gap *Phys. Rev.* B **70** 184526

[34] Labbé J and Friedel J 1966 Effect of temperature on the electronic instability and change in the crystal phase in low temperature V_3Si *J. Phys.* **27** 303

[35] Sadigh B and Ozolins V 1998 Structural instability and electronic excitations in Nb_3Sn *Phys. Rev.* B **57** 2793–800

[36] Weber W and Mattheiss L F 1982 Electronic structure of tetragonal Nb_3Sn *Phys. Rev.* B **25** 2270–84

[37] Shirane G and Axe J D 1971 Neutron scattering study of the lattice-dynamical phase transition in Nb_3Sn *Phys. Rev.* B **4** 2957–63

[38] Mattheiss L F and Testardi L R 1978 Plasma energies for A-15 compounds *Phys. Rev.* B **17** 4640–3

[39] Allen P B, Pickett W E, Ho K M and Cohen M L 1978 Anomalous resistivities of A15 metals—insights from band theory *Phys. Rev. Lett.* **40** 1532–4

[40] Allen P B, Beaulac T P and Khan F S 1986 DC transport in metals *Phys. Rev.* B **34** 4331–3

[41] Allen P B, Pickett W E and Krakauker H 1988 Anistropic normal-state transport properties predicted and analyzed for high-T_c oxide superconductors *Phys. Rev.* B **37** 7482–90

[42] Pickett W E and Allen P B 1973 Optical properties of Nb_3Sn: a probe of the electronic density of states *Solid State Commun.* **12** 677–80

[43] Lim K C, Thompson J D and Webb G W 1983 Electronic density of states and T_c in Nb_3Sn under pressure *Phys. Rev.* B **27** 2781–7

[44] Kartha S, Krumhansl J A, Sethna J P and Wickham L K 1995 Disorder-driven pretransitional tweed pattern in martensitic transformations *Phys. Rev.* B **52** 803–21

[45] Goringe M J and Valdre U 1966 Transmission electron microscopy of vanadium–silicon (V_3Si) at low temperatures *Proc. R. Soc.* A **295** 192–216

[46] Onozuka T, Ohnishi N and Hirabayashi M 1988 Low temperature electron microscopy on the cubic-tetragonal transformation of V_3Si *Met. Trans.* A **19A** 797–801

[47] Axe J D and Shirane G 1973 Inelastic-neutron-scattering study of (111) LA phonons in Nb_3Sn *Phys. Rev.* B **28** 4829–30

[48] Pintschovius L, Takei H and Toyota N 1985 Phonon anomalies in Nb_3Sn *Phys. Rev. Lett.* **54** 1260–3

[49] Hellman F and Geballe T 2005 Specific heat of thin-film A15 superconductors: an anomalous inhomogeneity discovered *Phys. Rev.* B **36** 107–20

[50] Mentink M G T, Bonevich J E, Dhalle M M J, Dietderich D R, Godeke A, Hellman F and ten Kate H H J 2013 Superconductivity in Nb–Sn thin films of stoichiometric and off-stoichiometric compositions *IEEE Trans. Appl. Supercond.* **23** 7100505

[51] Godeke A 2006 A review of the properties of Nb_3Sn and their variation with A15 composition, morphology and strain state *Supercond. Sci. Technol.* **19** R68–80
[52] Flükiger R 2003 Growth of A15 type single crystals and polycrystals and their physical properties *Handbook of Superconducting Materials* vol 1 (Bristol: IOP Publishing)
[53] Moore D F, Zubeck R B and Rowell J M 1979 Energy gaps of the A-15 superconductors Nb_3Sn,V_3Si, and Nb_3Ge measured by tunneling *Phys. Rev.* B **20** 2721–38
[54] Rudman D A, Hellman F, Hammond R H and Beasley M R 1984 A15 Nb–Sn tunnel junction fabrication and properties *J. Appl. Phys.* **55** 3544–53
[55] Ginzburg V L and Landau L D 1950 *Zh. Eksp. Teor. Fiz.* **20** 1064
[56] Abrikosov A A 1957 *Zh. Eksp. Teor. Fiz.* **32** 1442
[57] Gorkov L P 1959 *Zh. Eksp. Teor. Fiz.* **36** 1918
[58] Gennes P G De 1999 *Superconductivity of Metals And Alloys* (New York City: Perseus Books)
[59] Helfand E and Werthamer N R 1964 Temperature and purity dependence of the superconducting critical field, H_{c2} *Phys. Rev. Lett.* **13** 686–8
[60] Helfand E and Werthamer N R 1966 Temperature and purity dependence of the superconducting critical field, H_{c2}. II *Phys. Rev.* **147** 288–94
[61] Hohenberg P C and Werthamer N R 1967 Anisotropy and temperature dependence of the upper critical field of type-II superconductors *Phys. Rev.* **153** 493–7
[62] Werthamer N R, Helfand E and Hohenberg P C 1966 Temperature and purity dependence of the superconducting critical field, H_{c2}: III. Electron spin and spin–orbit effects *Phys. Rev.* **147** 295–302
[63] Schopohl N and Scharnberg K 1981 Upper critical fields in the presence of electron-spin and spin–orbit effects *Physica* B **107** 293–4
[64] Rieck C T, Scharnberg K and Schopohl N 1991 Quasiclassical theory of the upper critical field of high-field superconductors. Application to momentum-dependent scattering *J. Low Temp. Phys.* **84** 381–464
[65] Schopohl N and Scharnberg K 1985 Effect of anisotropic scattering on the upper critical field of high-field superconductord *Physica* B **135** 482–5
[66] Orlando T P and Beasley M R 1981 Pauli limiting and the possibility of spin fluctuations in the A15 superconductors *Phys. Rev. Lett.* **46** 1598–601
[67] Werthamer N R and McMillan W L 1967 Temperature and purity dependence of the superconducting critical field H_{c2}: IV. Strong-coupling effects *Phys. Rev.* **158** 415–7
[68] Masharov N F 1974 Properties of superconductors with strong coupling close to their critical temperature in arbitrary magnetic fiedlds *Fiz. Tverd. Tela* **16** 2343–9
[69] Schossmann M and Schachinger E 1986 Strong-coupling theory of the upper critical magnetic field H_{c2} *Phys. Rev.* B **33** 6123–31
[70] Schossmann M and Schachinger E 1984 Theory of H_{c2} for superconductors with energy-dependent electronic density of states *Phys. Rev.* B **30** 1349–56
[71] Godeke A, Jewell M C, Fischer C M, Squitieri A A, Lee P J and Larbalestier D C 2005 The upper critical field of filamentary Nb_3Sn conductors *J. Appl. Phys.* **97** 093909
[72] Mentink M G T, Dhalle M M J, Dietderich D R, Godeke A, Goldacker W, Hellman F, ten Kate H H J, Sumption M D and Susner M A 2012 The effect of Ta and Ti additions on the strain sensitivity of bulk niobium–tin *Phys. Proc.* **36** 491–6
[73] Jewell M C, Godeke A, Lee P J and Larbalestier D C 2004 The upper critical field of stoichiometric and off-stoichiometric bulk, binary Nb_3Sn *Adv. Cryog. Eng.* **711** 474–84
[74] Foner S and McNiff E J Jr 1981 Upper critical fields of cubic and tetragonal single crystal and polycrystalline Nb_3Sn in DC fields to 30 T *Solid State Commun.* **39** 959–64
[75] Naus M 2002 Optimization of internal-Sn Nb_3Sn composites *PhD Thesis* University of Wisconsin–Madison
[76] Fetter A L and Hohenberg P C 1969 Theory of type II superconductors *Superconductivity* vol 2 (New York: Marcel Dekker)
[77] Larbalestier D C 2015 private communication
[78] Bennemann K H and Garland J W 1972 Theory for superconductivity in d-band metals *AIP Conf. Proc.* **4** 103–37